Rewiring of the TCR signalosome in natural intestinal Intraepithelial T lymphocytes drives non-deletional tolerance

Watt, Harriet J.; Chawla, Amanpreet Singh; Lamoliatte, Frederic; Pryde, Sara; Knatko, Elena; Rasmussen, Kasper D.

DOI:
10.1101/2023.09.01.555859

Publication date:
2023

Title: Rewiring of the TCR signalosome in natural intestinal Intraepithelial T lymphocytes drives non-deletional tolerance

Authors: Harriet J. Watt[1], Amanpreet Singh Chawla[1], Frederic Lamoliatte[1], Sara Pryde[1], Elena Knatko[2], Kasper D. Rasmussen[2], David Bending[3], Mahima Swamy[1*]

Affiliations:

[1]MRC Protein Phosphorylation and Ubiquitylation Unit, University of Dundee; Dundee, DD1 5EH, United Kingdom.

[2]Division of Molecular, Cell and Developmental Biology, University of Dundee; Dundee DD1 5EH, United Kingdom.

[3]Institute of Immunology and Immunotherapy, University of Birmingham; Birmingham, United Kingdom.

*Address correspondence to: Dr. Mahima Swamy, Email: m.swamy@dundee.ac.uk

Running title: TCR signalosome rewiring in natural T-IEL

Keywords: Agonist selection; Intraepithelial T lymphocytes; antigen receptor signaling; phosphoproteomics; autoreactive T cells

Abstract

Intraepithelial T lymphocytes (T-IEL) are a large population of cytotoxic T cells that protect the small intestinal epithelium against pathogens. Based on ontogeny, T-IEL can be categorized into two major subsets: induced and natural. Natural T-IEL are agonistically selected in the thymus on self-antigens before migrating directly to the small intestine. Despite having self-reactive T cell antigen receptors (TCR), natural T-IEL are maintained in a tolerized state in the gut by unknown mechanisms. We therefore investigated TCR signaling in T-IEL using multiplexed fluorescent cell barcoding, phosphoproteomics and TCR signaling reporter mouse models, which revealed that TCR signaling is intrinsically suppressed in natural, but not induced, T-IEL. Unexpectedly, we discover that this cell intrinsic suppression was mediated through altered TCR signalosome components. Specifically, downregulation of the key signaling adaptor, Linker for activation of T cells (LAT) during thymic selection is a vital checkpoint for the development and tolerization of natural IELs. Thus, TCR signaling is rewired in self-reactive natural T-IEL to promote tolerance and prevent inappropriate inflammation in the gut.

One sentence summary: Self-reactive natural intestinal intraepithelial T lymphocytes are developmentally tolerized by rewiring the T cell antigen receptor signaling pathway through the downregulation of the adaptor protein, LAT.

Main Text:

Introduction

T cell development in the thymus involves a highly coordinated selection process that ensures functional T cell antigen receptor (TCR) binding to the major histocompatibility complex (MHC) while eliminating those T cells that strongly bind to self-peptides. This elimination, known as negative selection, prevents the maturation of autoreactive T cells. Upon exiting the thymus, T cells require activation through their TCR to drive their subsequent differentiation and to perform effector functions. However, a small subset of T cells in the thymus escape negative selection, potentially due to lack of co-stimulation during the strong binding and activation of their TCRs to self-ligands (*1*). These self-reactive T cells undergo a process of agonist selection, leading to clonal diversion into specialized lineages, including natural regulatory T cells (Tregs), invariant natural killer T cells (NKT), and natural intestinal intraepithelial T cells (T-IEL) (*2*). While Tregs are known to require their TCR for function in the periphery, and NKT cells are also activated through their TCR (*3,4*), little is known about the role of the TCR is on agonist-selected TCRαβ T-IEL.

T-IEL are a diverse population of T cells that reside in the epithelial layer of the small intestine. They are involved in the recognition of foreign antigens and repair of damaged epithelium. Based on their ontogeny, T-IEL are comprised of two main populations, induced and natural. Induced T-IEL express the αβ TCR and either the CD4 or CD8αβ coreceptors, and proceed through classical T cell development, transiting through positive and negative selection processes and exiting the thymus as naïve $CD4^+$ or $CD8^+$ T cells. In the periphery, these cells encounter their cognate antigen and upregulate gut-tropic molecules that facilitate the migration into the small intestine (*5*).

Natural T-IEL express either αβ or γδ TCRs and are defined by the expression of the CD8αα coreceptor, which they upregulate upon entry into the gut. Natural γδT-IEL develop from $CD4^-$ $CD8^-$ double negative (DN) thymocytes where expression of the TCR diverts these cells to γδ T cell development. TCR$\gamma\delta^+$ T cells exit the thymus in a naïve state, and enter gut-associated lymphoid tissue, such as mesenteric lymph nodes and Peyer's patches, where they can become activated, proliferate and selected to move into the epithelial layer of the gut to mature into γδT-IEL (*6*). In contrast, natural αβT-IEL develop similarly to induced T-IEL,

proceeding through DN stages, β-selection and upregulation of CD4 and CD8 coreceptors to become double positive (DP) thymocytes. The development of natural αβT-IEL precursors then deviates from conventional T cells. Natural T-IEL precursors have a TCR that reacts strongly towards self-antigen (*7–9*), but instead of being deleted, these cells differentiate into T-IEL progenitors, in a process known as agonist selection. Strong TCR signals induced by the self-antigens drive the upregulation of CD5, PD-1 and CD69, and the downregulation of CD4 and CD8 (*10*). These agonistically selected cells further mature by upregulating gut tropic molecules and CD122, and are trafficked into the epithelial layer of the small intestine (*11,12*). Thus, the TCR expressed on T-IEL precursors defines the developmental route these cells will take to the gut.

Signaling pathways downstream of the TCR in conventional T cells have been well elucidated. Briefly, antigen binding to the TCR induces phosphorylation of immunoreceptor tyrosine-based activation motifs (ITAMs) on the associated CD3 chains by the Src protein kinase, Lck. The tyrosine kinase zeta-associated protein 70 (ZAP-70) gets activated by binding to the phosphorylated ITAMs, and phosphorylates the transmembrane adaptor protein, linker for activation of T cells (LAT). Phosphorylated LAT acts as a central hub for signaling molecules, recruiting Vav, Itk, PLCγ1, Grb2, Gads and SLP-76, that then facilitates downstream signaling (*13*). While TCR signaling pathways in conventional $CD8^+$ T cells are well defined, the role of the TCR and its downstream signaling in T-IEL are less well understood. Natural T-IEL have impaired proliferative capacity upon stimulation through the TCR (*14*). The expression of the αβTCR on $CD4^+$ induced T-IEL is necessary for their differentiation and migration into the intraepithelial layer, but is not required for their maintenance (*15*). On the other hand, γδT-IEL were shown to be refractory to TCR stimulation (*16,17*), and showed high basal intracellular calcium levels. Interestingly, blockade of the γδTCR resulted in decreased basal calcium levels, suggesting that the γδTCR is constantly triggered *in vivo* (*16*). In this context, it is noteworthy that the $Vγ7^+$ TCR, that is expressed on 40-80% of γδT-IEL, interacts with butyrophilin-like (Btnl) molecules, Btnl1 and Btnl6, expressed by intestinal epithelial cells (*18*). This TCR-driven interaction is necessary for the presence of the $Vγ7^+$ population, and could induce activation in these cells as measured by CD69 and CD25 expression. Thus $Vγ7^+$ T-IEL have a self-reactive TCR.

The antigen recognized by the TCR is also important in the development of TCRαβ$^+$CD8αα$^+$ T-IEL, as when the TCRs of natural T-IEL were sequenced and cloned back into progenitors, all T cells expressing the natural T-IEL TCR became TCRαβ$^+$CD8αα$^+$ T-IEL and migrated to the small intestinal epithelium (*11,19*). This demonstrates the requirement for specific TCR sequences on natural T-IEL that home to the gut. Interestingly, natural T-IEL have an altered TCR composition with the incorporation of the FcεR1γ chain instead of CD3ζ (*20,21*), and also express lower levels of LAT compared to conventional T cells (*22*), however it is not known whether these changes affect TCR signaling in T-IEL once they are in situ in the epithelium. Moreover, it is unclear how self-reactive T-IEL, such as TCRαβ$^+$CD8αα$^+$ T-IEL and Vγ7$^+$ TCRγδ T-IEL are maintained in the gut environment without causing autoimmunity.

Here, we investigate the role of TCR signaling in T-IEL in maintaining T-IEL tolerance by monitoring the phosphorylation of downstream signaling proteins. Our findings reveal that all natural T-IEL populations, TCRγδ$^+$ and TCRαβ$^+$, are refractory to TCR stimulus, compared to induced T-IEL and conventional peripheral CD8 T cells. We further establish that this loss of TCR responses is not due to the immunosuppressive environment or inhibitory receptor signaling, but rather due to global changes in the TCR signaling pathway in natural T-IEL as compared to conventional T cells. We find downregulation of key TCR signaling adaptor molecule, LAT, is the most proximal event that is required for both development and maintenance of tolerant T-IEL. Thus, downregulation of TCR signaling is an active process driving the tolerance of intestinal epithelium resident T cells.

Results

TCR signal transduction is suppressed in natural T-IEL

We first investigated the responses of T-IEL to TCR activation in comparison to conventional CD8$^+$ T cells derived from the lymph nodes. To allow us to stimulate both cell types in identical conditions, we developed a modified version of the fluorescent cell barcoding technique (*23*) to differentially label live T-IEL and conventional CD8$^+$ T cells. T-IEL were labelled with a Live/Dead dye and combined with unstained conventional CD8$^+$ T cells, allowing these cells to be stimulated in the same tube as T-IEL and subsequently differentiated from T-IEL during flow analysis (Suppl. Fig. 1A). The cells in the various stimulation conditions

were then subject to fluorescent cell barcoding prior to phospho-flow cytometry. The specificities of phospho-antibodies were confirmed using inhibitor-treated cells (Suppl. Fig. 1B). Both conventional $CD8^+$ T cells and the induced T-IEL subset ($TCR\alpha\beta^+CD8\alpha\beta^+$) showed strong responses to TCR stimulation, with >60% of cells positive for phosphorylation of ERK1/2 and the ribosomal protein S6 (Fig. 1A). In contrast, less than 15% of the agonist-selected natural T-IEL $TCR\alpha\beta^+CD8\alpha\alpha^+$ subset responded to TCR signals, and the other natural T-IEL $TCR\gamma\delta^+CD8\alpha\alpha^+$ subset also responded poorly (<40%). This differential activation upon stimulation through the TCR between induced and natural T-IEL subsets was seen for numerous signaling proteins, as illustrated in the heatmap depicting the $\log_2$ fold change of the median fluorescence intensity (MFI) (Fig. 1B).

It is possible that despite low activation of the signaling pathways, a lower threshold of activation allows T-IEL to respond functionally to TCR triggering. However, we found that both natural T-IEL populations produce less IFNγ, and show reduced expression of CD107, a marker of degranulation, compared to the induced T cells when stimulated with plate-bound anti-CD3 directly after isolation (Fig. 1C). Thus, the decreased phosphorylation of key signaling nodes seen in natural T-IEL also translated into reduced functional responses of natural T-IEL, particularly the agonist-selected $TCR\alpha\beta^+CD8\alpha\alpha^+$ subset, confirming that natural T-IEL are refractory to TCR stimulation.

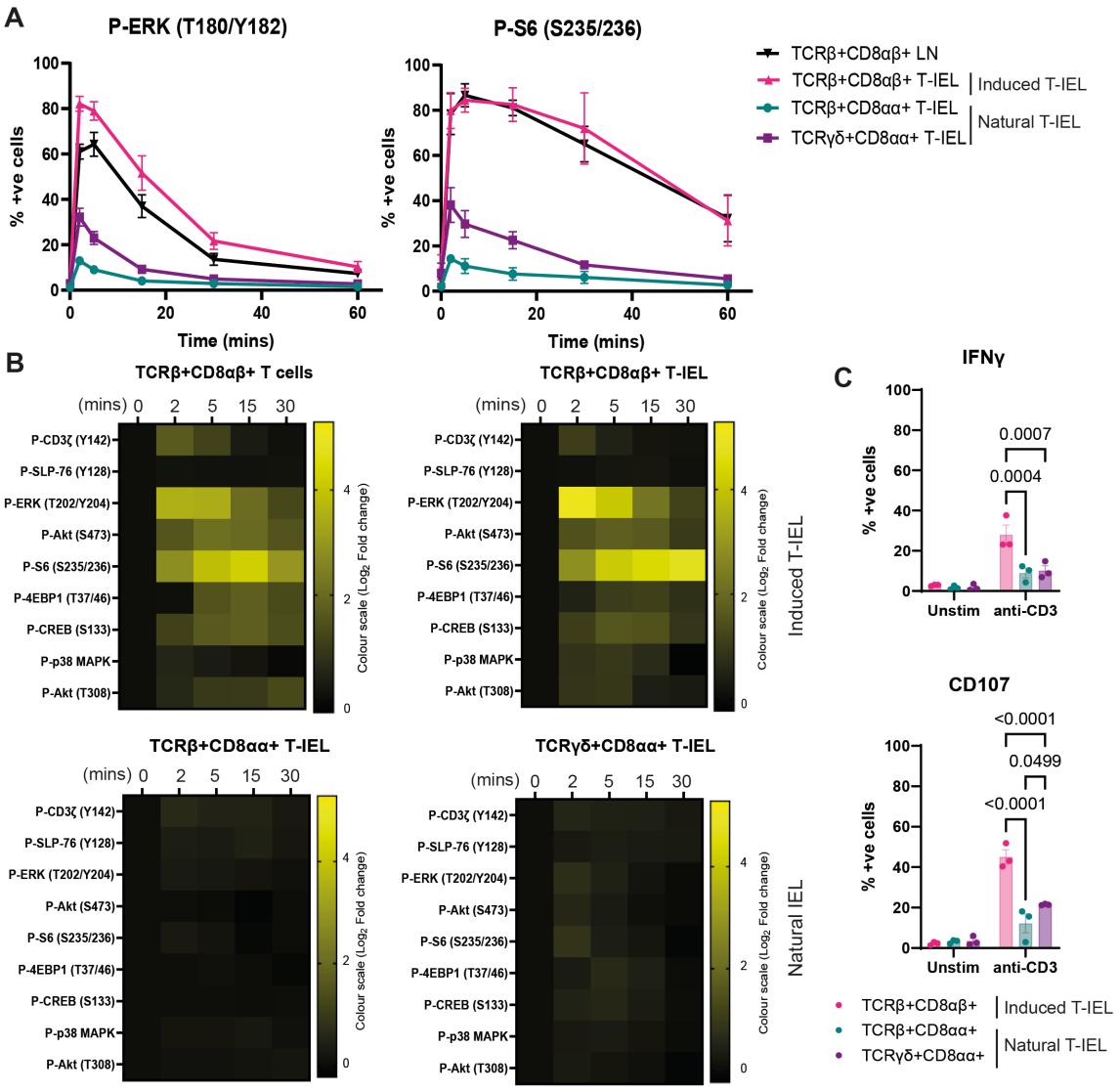

Figure 1: TCR signaling is suppressed in natural T-IEL. (A) Percentage of cells that are positive for phosphorylation of ERK and S6 after stimulation with anti-CD3 (30 µg/ml) crosslinked with anti-Hamster (5 µg/ml). Data show the mean and SEM of 5 independent experiments. (B) Heatmaps depict $\log_2$ fold change of mean MFI of phospho-proteins in T-IEL subsets and conventional TCRαβ$^+$CD8αβ$^+$ cells after stimulation with anti-CD3 (30 µg/ml) crosslinked with anti-Hamster (5 µg/ml). Fold change is calculated relative to the unstimulated condition. Data are the mean of at least 3 independent experiments. (C) Percentage of T-IEL that are positive for IFNγ and CD107 upon stimulation with plate-bound anti-CD3 (3 µg/ml). Data represents mean and SEM of 3 replicates. Statistical significance is calculated by ANOVA and Tukey's post hoc correction.

Natural T-IEL display features of strong TCR stimulation

A previous study (*16*) had suggested that γδT-IEL are hyporesponsive to TCR-induced calcium flux in vitro, as they are undergoing constant TCR triggering *in vivo*, that drives a high basal calcium in intestinal T-IEL

compared to peripheral lymphocytes. To investigate steady-state signaling in T-IEL, we compared the ex vivo baseline phosphorylation of signaling proteins in T-IEL subsets to conventional T cells isolated from lymph nodes (LN). All intestinal T-IEL populations had increased phosphorylation of signaling proteins at steady-state compared to LN T cells (Fig. 2A). Interestingly, the pattern of basal phosphorylation appears to be different in natural αβ T-IEL, compared to the other two T-IEL populations, with higher phosphorylation of TCR-proximal proteins CD3ζ and SLP-76 in natural αβ T-IEL, and lower basal S6 phosphorylation. These data suggested that T-IEL may indeed be undergoing continuous antigen receptor signaling in vivo.

To further investigate this homeostatic activated state of T-IEL, we made use of the transgenic reporter *Nr4a3*-Tocky mouse (*24*). In this model a fluorescent timer protein (*25*) is expressed under the control of the TCR inducible gene *Nr4a3*, which is an NFAT-responsive gene that is induced in response to strong and sustained TCR signals (*26*). Initially upon translation the Timer protein has blue fluorescence before undergoing irreversible maturation to a red fluorescent form with an approximate blue half-life of 4 hours and red half-life of >10 days (Fig. 2B). This model can therefore reveal when the TCR has been recently active in cells, and cells undergoing constant TCR signaling would be expected to have a high Timer-blue signal. Over 70% of natural T-IEL were highly positive for Nr4a3-Red at homeostasis (Fig. 2C and Suppl. Fig. 2A), indicative of strong TCR stimulation at some point in these cells. This proportion was significantly higher in natural T-IEL than in induced T-IEL (20%) and conventional CD8 T cells (<10%) from mesenteric lymph nodes (mLN) and spleen (Fig.2C). Very few T cells were positive for the Timer-blue signal (Fig. 2D). Strikingly, the natural γδ and αβ T-IEL populations had a significantly higher percentage (3 - 8%) of Nr4a3-Blue positive cells compared to induced T-IEL and peripheral T cells, indicative of very recent TCR stimulation (<4 hours) of a subset of natural T-IEL. These findings suggested that natural T-IEL are experiencing strong, yet sporadic TCR signals *in vivo*, not constant activation. It is probably these short TCR signals that sustain the high Timer-red expression in the natural T-IEL and explains the higher basal phosphorylation of signaling proteins in the aggregated population-based data in Fig. 2A. These data indicate that natural T-IEL are not undergoing continuous TCR triggering at the intestinal epithelium, thus continuous activation cannot explain the lack of TCR responses in these cells.

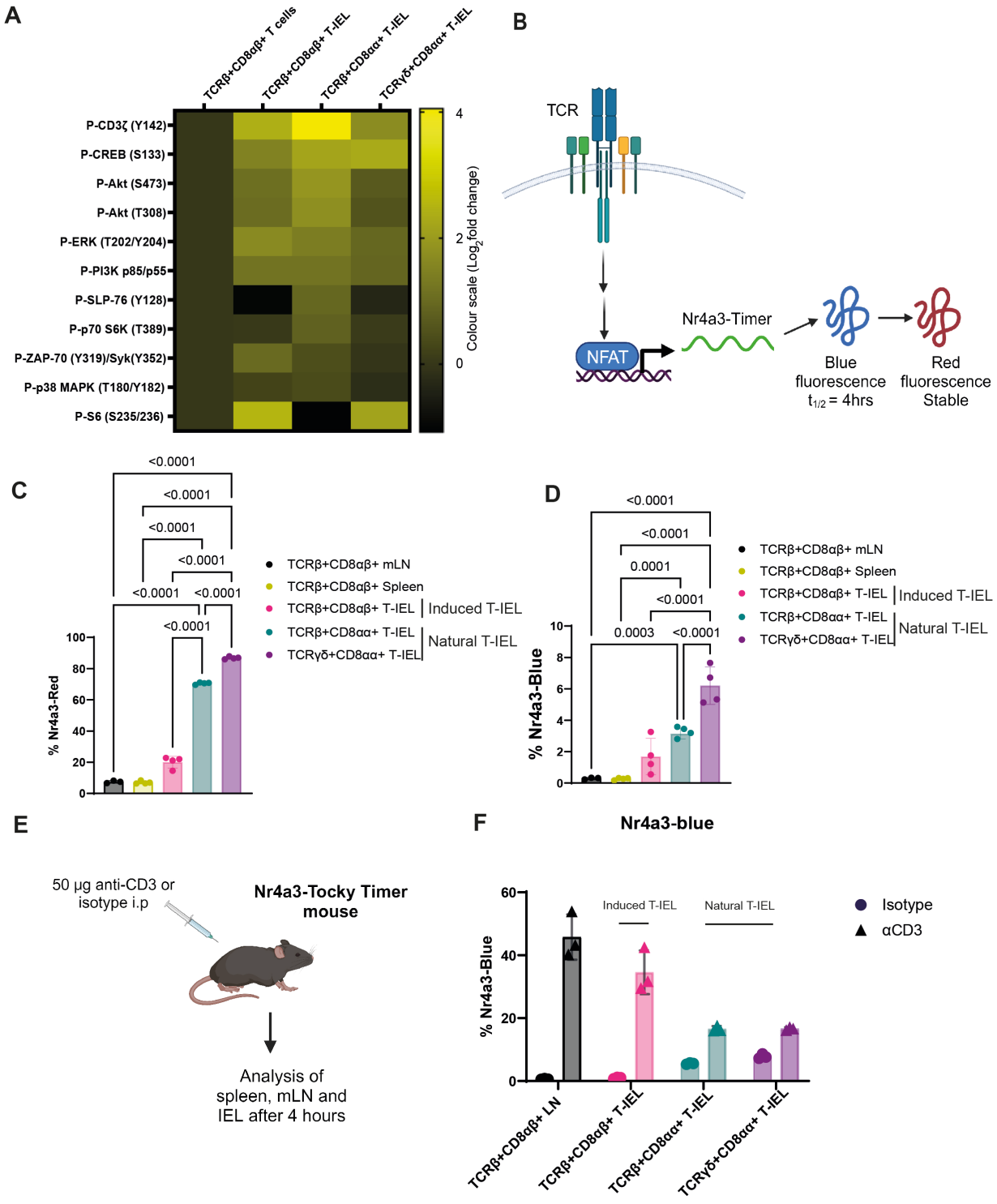

Figure 2: Natural T-IEL display features of historic TCR stimulation but are hyporesponsive to in vivo stimulation. (A) Heatmap depicts log_2fold change of mean MFI of phospho-protein in T-IEL subsets at basal levels relative to TCRαβ$^+$CD8αβ$^+$ conventional T cells. Data are mean of at least 3 independent experiments. (B) Schematic description of the Nr4a3-Tocky reporter. (C) Plots of percentage of cells that are positive for Nr4a3-Red and (D) Nr4a3-Blue in mLN, spleen and T-IEL cell subsets, respectively. Data shows mean and SEM of 4 replicates. Statistical significance is calculated by ANOVA and Tukey's post hoc test. (E) Schematic of *in vivo* stimulation experimental design. (F) Percentage of cells positive for Nr4a3-Blue 4 hours after intraperitoneal injection with 50 µg anti-CD3 or isotype antibody. Data show the mean and SEM of 3 replicates.

The role of tissue environment and inhibitory receptors in T-IEL TCR responses

Natural T-IEL do not express CD28, however other receptors on T-IEL could potentially provide costimulatory signals *in vivo* (*27*). We therefore used the Nr4a3-Tocky model to test the response of T-IEL to TCR stimulation *in vivo* where potential costimulatory signals could be present. Nr4a3-Tocky timer mice were injected intraperitoneally with anti-CD3 or an isotype antibody and T cells in the spleen, mLN and gut were analyzed after 4 hours (Fig. 2E). While there was a robust increase in Nr4a3-blue in splenic and LN T cells in mice that had been injected with anti-CD3, less than 20% of natural T-IEL expressed Nr4a3-blue upon the same stimulus (Fig. 2F and Suppl. Fig. 2B). This *in vivo* response mirrors the decreased response of natural T-IEL observed *ex vivo* (Fig. 1). Thus, hyporesponsiveness of natural T-IEL is maintained within the context of the gut environment.

The gut is a highly immunosuppressive environment, with cytokines such as TGFβ and IL-10 in abundance. Hence, we next tested whether removing T-IEL from the immunosuppressive environment of the gut, would allow T-IEL to respond to TCR signals. T-IEL were purified and cultured with IL-15-receptor complexes for 4 days, before stimulating the cells with anti-CD3. IL-15 was added to maintain cell survival. Despite removing natural T-IEL from the gut environment, and in the absence of any other cells that might provide suppressive signals, we did not see an increase in TCR-triggered phosphorylation of signaling proteins in natural T-IEL (Suppl. Fig. 3A). However, induced T-IEL still showed robust responses to TCR triggering.

We also considered whether inhibitory receptor signaling might be important for suppressing T-IEL responses. T-IEL have previously been shown to express T cell inhibitory receptors, such as LAG-3 and 2B4 (Brenes, Vandereyken et al. 2021). These receptors are also expressed in exhausted T cells that are refractory to TCR stimulation (*28*), and blocking LAG-3 can rejuvenate exhausted T cell responses. Further, LAG-3 was recently shown to suppress TCR signaling by blocking the very first step of Lck recruitment to the TCR (*29*). To test if LAG-3 played any role in suppressing T-IEL function, T-IEL were cultured with or without anti-LAG-3 blocking antibodies for 96 hours, before stimulation with crosslinked anti-CD3. However, there was no difference in response to anti-CD3 stimulation between cells cultured with or without the LAG-3 antibody (Suppl. Fig. 3B), and natural T-IEL still maintained their hyporesponsive state. As a control, we checked that

culture with anti-LAG-3 decreased the expression of the LAG-3 receptor, indicating the antibody had bound (Suppl. Fig. 3C). Overall, these data indicate that the lack of natural T-IEL responses to TCR triggering was not due to lack of co-stimulation, nor due to immunosuppression by cytokines or inhibitory receptors in the environment of the gut. Taken together, the data presented so far suggests that IEL hyporesponsiveness to anti-CD3 stimulation is cell-intrinsic.

Natural T-IEL respond to stimulation with TCR signaling mimetics

Phorbol myristate acetate (PMA) with Ionomycin are often used to mimic TCR signaling, as they biochemically activate the main signaling pathways of the TCR. PMA activates protein kinase C (PKC) (*30*); ionomycin is a calcium ionophore that stimulates calcium flux (*31*), thus triggering the TCR signaling pathways downstream of phospholipase-Cγ (PLCγ) and PKC. We tested whether these TCR mimetics that bypass TCR ligation with antigen could trigger signaling in T-IEL to check if the signaling pathways downstream of PLCγ were intact in T-IEL. Indeed, we found that PMA and ionomycin induced phosphorylation of ERK1/2 in 100% of T-IEL subsets, and also induced strong phosphorylation of p38 and CREB in T-IEL similar to conventional CD8 T cells (Fig. 3A, C, Suppl. Fig. 4). These data indicate that the pathways downstream of PLCγ and PKC are intact in natural T-IEL as well as in induced T-IEL and CD8 T cells.

Since signaling pathways downstream of PLCγ and PKC were intact, we explored the functionality of the TCR proximal signaling proteins. Pervanadate is a pan-tyrosine phosphatase inhibitor that mimics TCR stimulus by inhibiting TCR proximal phosphatases such as CD45, triggering strong activation of the TCR proximal kinases, Lck and ZAP70 (*32*). Pervanadate induced phosphorylation of ERK and Akt in all T-IEL subsets (Fig. 3A) but was not able to drive phosphorylation of S6, CREB, 4EBP1 or p38 MAPK in the natural T-IEL subsets (Fig. 3A-C). Moreover, the intensities of phosphorylation of ERK and Akt were lower in natural T-IEL (Fig. 3B) as compared to induced T-IEL. These data indicate a disruption in TCR signal transduction in natural T-IEL, where the connection to some pathways, such as ERK and Akt, are partially preserved and other pathways are disconnected. This disruption appears to be at the TCR proximal stage of the signaling pathway, since PMA, but not pervanadate, could restore ERK1/2, S6, and CREB phosphorylation. Alternatively, the TCR in natural T-IEL connects to different signaling pathways as compared to that seen in conventional T cells.

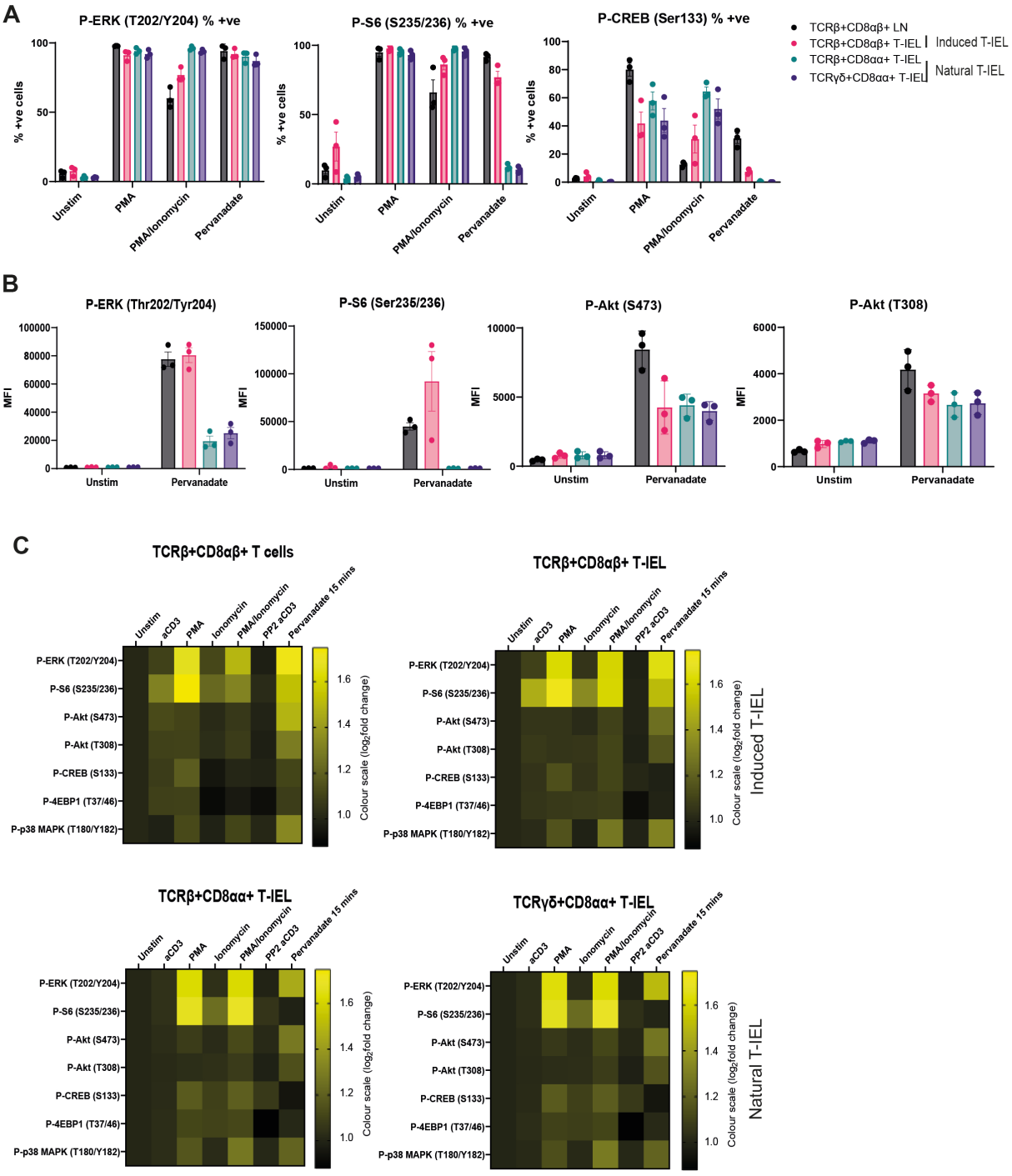

Figure 3: All T-IEL subtypes can be activated by PMA and Ionomycin. Bar plots depicting the (A) percentage of cells that are positive for phosphorylation of signalling proteins or (B) MFI of phospho-proteins upon stimulation with anti-CD3 (30 µg/ml) crosslinked with anti-Hamster (5 µg/ml), PMA (100 ng/ml), Ionomycin (1 µg/ml) or pervanadate (10 µM). 10 µM PP2 was added to the indicated condition and incubated for 1 hour prior to stimulation. Data represent the mean and SEM of 3 independent replicates. (C) Heatmaps depict the log_2fold change of mean MFI of the phospho-proteins in T-IEL subsets and conventional CD8 T cells under the same stimulation conditions as (A). Fold change is calculated relative to the unstimulated condition. Data represent the mean of 3 independent experiments.

Phosphoproteomics reveals modified TCR signalosome in natural T-IEL

To conduct a broader exploration of the signaling pathways induced by pervanadate in natural T-IEL, we stimulated pooled αβ and γδ CD8αα$^+$ T-IEL and conventional CD8$^+$ T cells with pervanadate. Tyrosine-phosphorylated proteins were pulled down using high affinity SH2 superbinder beads that specifically bind to phospho-tyrosines (*33,34*). Immunoblotting of the purified proteins with anti-phosphotyrosine revealed a different pattern of tyrosine-phosphorylated proteins in CD8α$^+$ natural T-IEL as compared to conventional CD8 T cells (Fig. 4A). To identify these differentially phosphorylated proteins we conducted phospho-proteomic analysis of tyrosine-phosphorylated peptides isolated from natural T-IEL (CD8α$^+$ CD8β$^-$ CD4-) and LN CD8$^+$ T cells. Approximately 10x10^6 natural T-IEL were sorted from the pooled T-IEL populations from 10 mice and the same number of conventional CD8$^+$ T cells purified from lymph nodes and spleens for each replicate (Suppl. Fig. 5). The natural T-IEL population used for phospho-proteomic analyses consisted of both αβ and γδ T-IEL, as enough cells could not be obtained for the individual populations. For the same reason, induced T-IEL, which are much fewer compared to natural T-IEL, were not used in these analyses. However, since induced T-IEL respond similarly to TCR stimulation as conventional CD8 T cells, we assume similar signaling pathways are triggered in both cell types. Cells were stimulated with pervanadate for 5 minutes before being subject to phospho-proteomics workflow. Samples were lysed, digested, labelled using Tandem Mass Tagging, pooled and tyrosine-phosphorylated peptides purified using SH2 superbinder beads (Fig. 4B). In total we identified 819 phospho-peptides in the T-IEL and lymph node T cells, that were confirmed phospho-tyrosine containing peptides, in the first phospho-proteomic analyses of intestinal T-IEL. Principal component analyses revealed that phosphopeptides from T-IEL and LN CD8 T cells cluster away from each other and the majority of the difference is explained by the differences in cell type (Fig. 4C). Clustering the significantly regulated phospho-sites in a heatmap further corroborates large differences between natural T-IEL and lymph node samples, while showing good correlation between biological replicates (Fig. 4D, E).

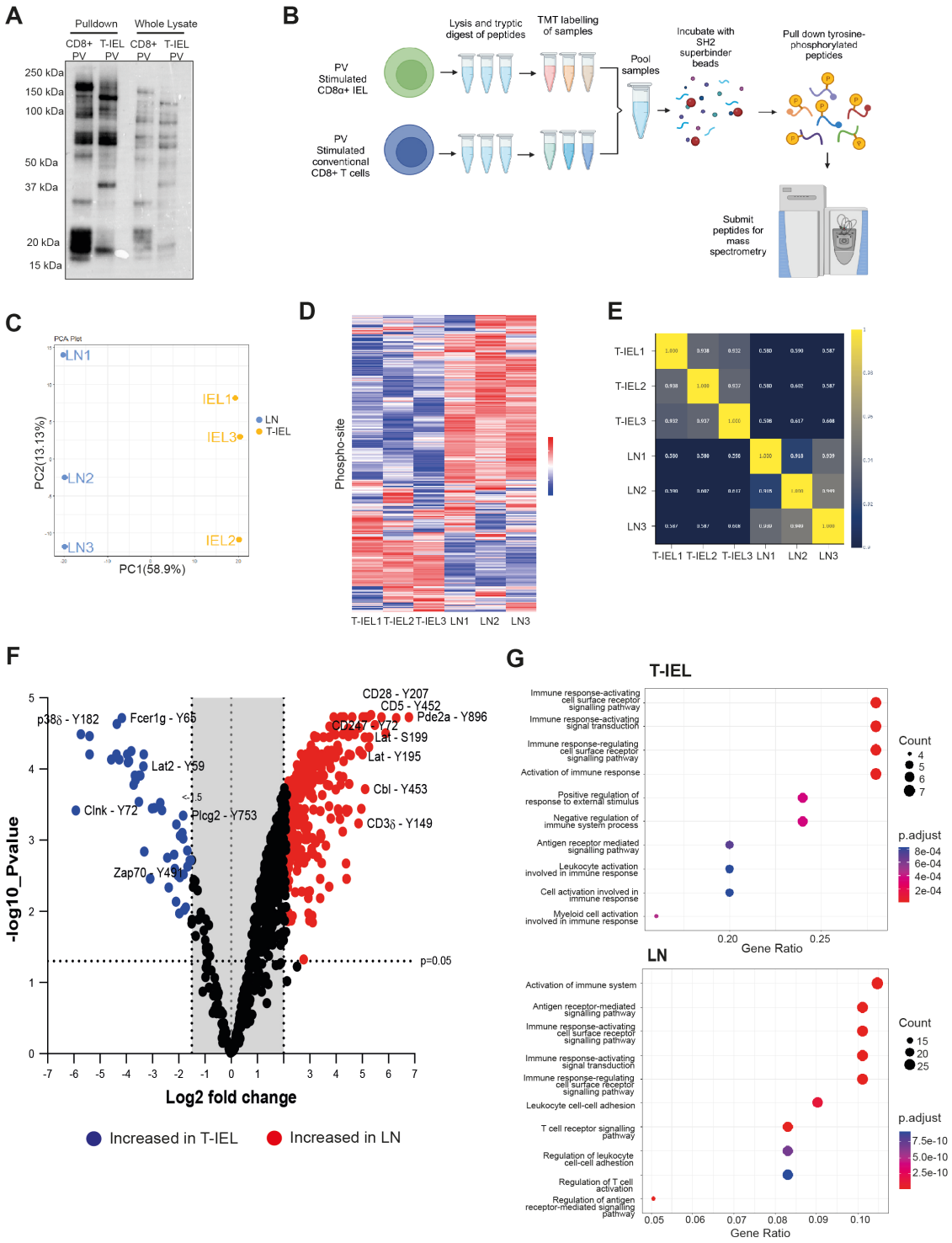

Figure 4: Phosphorylation of proteins is different in natural T-IEL compared to conventional CD8 T cells. (A) Phospho-tyrosine blot of lysates from pooled αβ and γδ natural T-IEL or conventional CD8+ T cells stimulated with pervanadate (10 µM) for 5 minutes and enriched for phosphorylated tyrosine proteins using SH2 superbinder beads. (B) Experimental procedure for the preparation of samples for phospho-proteomics. (C) PCA plot of T-IEL and LN CD8 T cell samples submitted for phospho-proteomics in (B). (D) Clustered heatmap of significantly regulated phospho-sites in natural T-IEL compared with LN CD8 T cells in (B). (E) Correlation heatmap of T-IEL and lymph node phospho-proteomic samples. (F) Volcano plot of $\log_2$ fold change and $\log_{10}$ p-value of the phospho-sites identified in the natural T-IEL and LN CD8 T cells. (G) GO term analysis of the proteins whose phospho-sites are most significantly upregulated in T-IEL and LN CD8 T cells.

Further investigation of the differentially phosphorylated peptides reveals overwhelmingly more proteins are phosphorylated in conventional CD8 T cells (570 phospho-sites) as compared to 60 phospho-sites significantly enriched in the natural T-IEL population (Fig. 4F). GO term analysis of the proteins that were significantly upregulated in either natural T-IEL or CD8 T cells confirm that pervanadate is very good at inducing antigen receptor signaling in conventional T cells, whereas in T-IEL, phosphoproteins involved in negatively regulating immune system processes and intriguingly, those associated with myeloid cells were enriched (Fig. 4G and Suppl. table 1). Interestingly, many of the phospho-peptides enriched in conventional CD8 T cells belong to proteins that are not expressed or are expressed at much lower levels in T-IEL. For example, CD28, CD5 and LAT (Linker for activation of T cells) are not expressed on natural T-IEL (Suppl. Fig. 6B), and TCR components CD3γ and CD3ζ (CD247), and other signaling molecules such as Themis, UBASH3A and PLCγ1 are expressed at very low levels (*27*). Conversely, peptides found highly phosphorylated in T-IEL belong to proteins that are exclusively expressed in natural T-IEL among T cells, including FcεR1γ, LAT2/NTAL, CLNK (Suppl. Fig. 6B). Interestingly, high mRNA expression of *FCER1G, LAT2, PLCG2, GCSAM*, *CLNK,* have also been shown to define a human natural T-IEL subset (*35*). From these overview analyses, it is clear that the signaling pathways induced in T-IEL downstream of the TCR differ significantly from those seen in classical TCR signal transduction in LN $CD8^+$ T cells, and many of these differences appear to correlate with differential protein expression.

Negative regulators of TCR signaling do not dampen the TCR response of natural T-IEL

From the phospho-proteomic experiments we see that the TCR signalosome and related proteins are altered in natural T-IEL potentially explaining the hyporesponsive phenotype. Natural T-IEL showed higher phosphorylation of several negative regulators of TCR signaling, including receptors (CD200R1, 2B4/CD244 (*36*)), adaptors (DOK1 (*37*), LAT2 (NTAL, non-T cell activation linker (*38*)), and tyrosine phosphatases (SHP-1 (encoded by *Ptpn6*) and SHP-2 (encoded by *Pptn11*)) compared to LN $CD8^+$ T cells (Suppl. Fig. 6). SHP-1 and SHP-2 can dephosphorylate CD3ζ and ZAP70, and are the key enzymes downstream of several inhibitory co-receptors expressed on T cells, such as CD5, PD-1 and SLAM (*39*). Further, these phosphatases were highly expressed in natural T-IEL (Suppl. Fig. 7A). To test if these phosphatases were involved in downregulating signaling in natural T-IEL, we knocked out either SHP-1 alone, or both SHP-1 and SHP-2 in T-IEL (Suppl. Fig.

7B). We stimulated T-IEL lacking either SHP-1 alone or both SHP-1 and SHP-2 with anti-CD3 and measured phosphorylation of ERK and S6 (Suppl. Fig. 7C). Surprisingly, we saw no difference in the response of any of the T-IEL populations to TCR stimulation in the absence of either SHP-1 or both SHP1/2. There was also no difference in the production of IFNγ in SHP-1/2-deficient T-IEL when the TCR was stimulated *in vivo* (Suppl. Fig. 7D). This led us to conclude that these phosphatases alone are not responsible for preventing signaling in natural T-IEL, or that there are other mechanisms in T-IEL that can compensate for the lack of these phosphatases.

Another key negative regulatory molecule expressed in natural T-IEL is NTAL/LAT2. Phosphorylation of LAT2 was significantly higher in natural T-IEL as compared to LN T cells (Fig. 5A). LAT2 is a transmembrane adaptor protein usually expressed in B cells and mast cells where it becomes phosphorylated after BCR or FcR ligation (*40,41*). Overexpression of LAT2 in T cells can suppress TCR signaling (*38,42*), potentially by sequestering signaling molecules away from LAT. Due to its high expression in natural T-IEL (Fig. 5B) we hypothesized that LAT2 was responsible for suppressing TCR signaling in these cells. We confirmed loss of expression of LAT2 in LAT2 KO γδ T-IEL (Supplementary Fig. 8A), and then showed that normal numbers of T-IEL were found in LAT2 KO mice (Suppl. Fig. 8B). Unexpectedly, stimulation of T-IEL from LAT2 KO mice showed no difference in phosphorylation of ERK and S6 in any of the T-IEL populations (Fig. 5C). However, after *in vivo* injection with anti-CD3, T-IEL in the LAT2 KO mice had significantly increased levels of IFNγ production from the natural αβ T-IEL subset (Fig. 5D) and increased TNFα production in both natural αβ and γδ T-IEL (Suppl. Fig. 8C). This difference is unique to natural T-IEL populations and was not observed in the splenic T cells where LAT2 is not expressed, indicating that there is a role for LAT2 in suppression of TCR signals in natural T-IEL. However, the effects were small, suggesting that LAT2 is only one of a suite of inhibitory mechanisms that suppress T-IEL. Alternatively, loss of key TCR signaling components in natural T-IEL may be more important than expression of negative regulators of signaling.

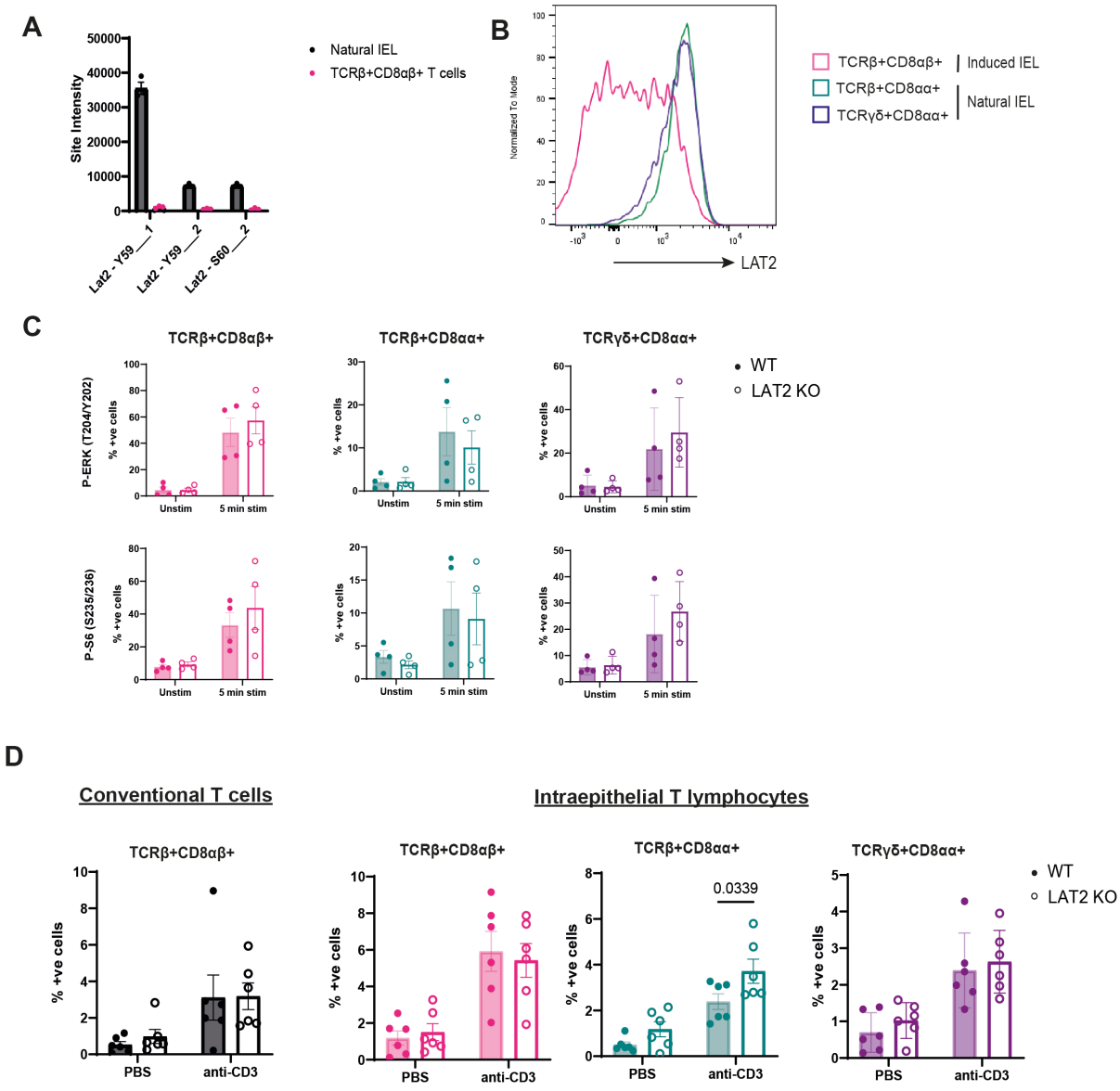

Figure 5: Response of LAT2 KO T-IEL to TCR stimulation. (A) Median imputed intensity of the phosphorylation of LAT2 in natural T-IEL and conventional TCR$\alpha\beta^{+}$CD8$\alpha\beta^{+}$ T cells upon stimulation with pervanadate, 10 µM. (B) Histograms of LAT2 expression in T-IEL subsets. (C) Graph of percentage of T-IEL subsets that are positive for phosphorylation of ERK and S6 after stimulation with anti-CD3 (30 µg/ml) crosslinked with anti-Hamster (5 µg/ml) in wild type (filles circles) and LAT2 KO (empty circles) T-IEL. (D) Graphs of the percentages of each subset of T-IEL or splenocytes that were positive for IFNγ after in vivo stimulation with anti-CD3 (50 µg) or PBS vehicle control for 3 hours in WT and LAT2 KO mice. Data shows mean and SEM of 6 replicates.

Forced expression of LAT in natural T-IEL rescues TCR signaling

The absence of negative regulators of TCR signaling, SHP-1, SHP-2 and LAT2, had minimal effect on the response of T-IEL to stimulation through the TCR. Linker for Activation of T cells (LAT) is an essential signaling

adaptor protein that links the TCR to downstream signaling components through the scaffolding of a multi-protein complex. From our phospho-proteomic analyses we noticed that natural T-IEL had significantly reduced phosphorylation of LAT at multiple tyrosine residues (Fig. 6A). Data mining our previous proteomic analyses, we found that natural T-IEL expressed lower/absent levels of the LAT protein than conventional TCRβ^+CD8$\alpha\beta^+$ T cells and induced T-IEL, (*43*) (Fig. 6B). This was confirmed by flow cytometry of LAT in mature T-IEL (Fig. 6C, Suppl. Fig. 9A). As LAT is essential for TCR signaling (*44,45*), absence of this central regulator could be the main reason that natural T-IEL are hyporesponsive to TCR stimulus. To test whether re-expression of LAT in natural T-IEL rescues TCR signaling, we retrovirally transduced LAT-IRES-GFP construct or GFP only into purified T-IEL and stimulated these cells with anti-CD3 after 7 days in culture. Viability of the T-IEL at this time was between 65-90% in all samples and LAT expression was restored in up to 15% of T-IEL (Fig. 6D). Importantly, we see that a significantly higher percentage of the natural, but not induced, T-IEL transduced with LAT, as compared to those transduced with GFP alone, responded to TCR triggering by increased phosphorylation of CREB, ERK, and pS6 (Fig. 6E and Suppl. Fig. 9C). Interestingly, human natural T-IEL were also found to express lower levels of LAT and higher levels of LAT2 by scRNA-seq compared to induced CD8$^+$ T-IEL (*46*) (Fig. 6F). Thus, a cell-intrinsic mechanism of loss of LAT that is conserved in humans regulates the TCR responses of natural T-IEL.

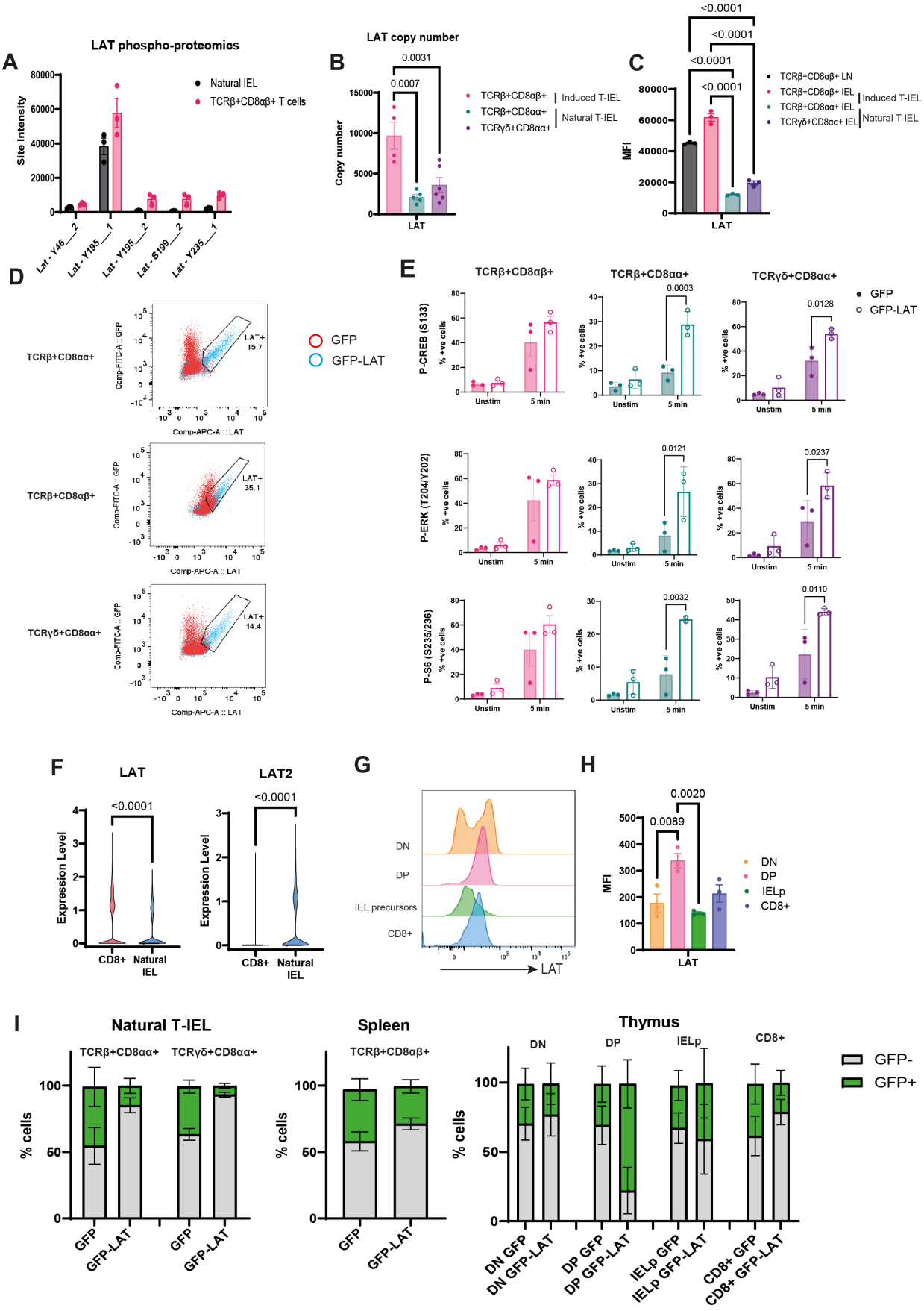

Figure 7: LAT is downregulated in natural T-IEL and in T-IEL precursors in the thymus. (A) Phosphorylation of LAT at indicated sites upon stimulation with pervanadate in natural T-IEL and conventional CD8 T cells from phosphoproteomics analyses. (B) Copy number of LAT in T-IEL subsets (Data from James et al, 2021). Statistical significance calculated by ANOVA and Tukey's post hoc correction (C) Flow cytometric expression of LAT in mature T-IEL subsets and LN CD8 T cells. Data shows mean and SEM of 3 independent replicates. Statistical significance calculated by t-test and Tukey's post hoc correction. (D) Representative dot plots of GFP and LAT expression in each T-IEL subset transduced with GFP (red) or LAT-IRES-GFP (blue) vectors. Gate shows percentage of LAT-positive cells. (E) Graph of the percentage of each T-IEL subset positive for phosphorylation of CREB, ERK or S6 at indicated sites when transduced with GFP empty vector (filled circles) or vector containing LAT (empty circles). Data shows mean and SEM of 3 replicates. Statistical significance is calculated by ANOVA and Tukey's post hoc correction. (F) Expression of LAT and LAT2 in human T-IEL subsets, either CD8+ (induced) or natural. P-value calculated using Mann-Whitney test. (G) Representative histogram and (H) graph of LAT expression in thymocyte populations, $CD4^{-}CD8^{-}$ (DN), $CD4^{+}CD8^{+}$ (DP), DN $TCR\beta^{+}CD5^{+}PD\text{-}1^{+}$ (IELp, see Suppl. Fig. 9B for gating strategy) and mature CD8 single positive thymocytes (CD8+). Data shows mean and SEM of 3 replicates. Statistical significance calculated by ANOVA and Tukey's post hoc correction. (I) Percentage of cells expressing GFP in natural T-IEL, spleen and thymic populations, 6 weeks after adoptive transfer of HSPCs transduced with either GFP or GFP-LAT, n=2 each.

Downregulation of LAT is a checkpoint for natural T-IEL development

To identify at which stage of development the downregulation of LAT expression in T-IEL occurs, we investigated the expression of LAT in the thymus. We see that post-selection T-IEL precursors in the thymus have low levels of LAT compared to double positive thymocytes from which they are derived (Fig. 6G, H, Suppl. Fig. 9B). These data suggest that downregulation of LAT is associated with the clonal diversion of DP thymocytes into T-IEL and may be a mechanism by which self-reactive TCRαβ thymocytes are tolerized during development, thus allowing their survival while preventing autoreactivity in the intestine.

We hypothesized that downregulation of LAT was either essential for the clonal diversion and development of T-IEL, or necessary for the tolerization of T-IEL once they enter the intestinal epithelium. To test these hypotheses, we retrovirally transduced hematopoietic stem and progenitor cells (HSPCs) with a LAT-IRES-GFP construct - that cannot be downregulated - and transplanted these into lethally irradiated mice. As a control, GFP alone was introduced into HSPCs (Suppl. Fig. 9D). While a similar percentage of GFP-only transduced HSPCs developed into natural T-IEL and into conventional $CD8^{+}$ T cells, HSPCs with forced expression of LAT did not differentiate into $TCR\alpha\beta^{+}CD8\alpha\alpha^{+}$ T-IEL or $TCR\gamma\delta^{+}CD8\alpha\alpha^{+}$ T-IEL although they

differentiated into conventional CD8 T cells (Fig. 6I). As a positive control, we show that forced expression of LAT also blocked B cell development (Suppl. Fig. 9E), indicating that expression of LAT, that is normally not expressed in B cells, inhibits the B cell development program. Thus, downregulation of LAT expression in self-reactive T-IEL precursors in the thymus is necessary for the development and clonal diversion of natural T-IEL, and the loss of LAT is responsible for the reduced response of natural T-IEL to TCR stimulation.

Discussion

The presence of self-reactive T cells outside the thymus necessitates that their self-reactivity be controlled, either through active immunosuppression by regulatory T cells or by induction of anergy. Loss of functional TCR responses is often defined as anergy, yet how T cells stop responding through their TCR from a signal perspective, and whether the same mechanisms are utilized by all TCR-non-responsive T cells is not clear. Here we reveal that both TCRαβ$^+$CD8αα$^+$ and TCRγδ$^+$CD8αα$^+$ self-reactive T-IEL populations drastically reduce TCR responsiveness via cell-intrinsic remodeling of the TCR signalosome. Likely occurring during thymic development, this remodeling involves key modifications like the downregulation of the central TCR signaling adaptor protein LAT, and the concomitant upregulation of NTAL/LAT2 expression, thus switching off TCR signals. This provides an answer to the long-standing question of how self-reactive T cells escape negative selection and are clonally diverted to the gut, as this loss of TCR activity permits natural T-IEL to tolerate any self-ligands that might be present.

When does this rewiring of the TCR signalosome occur? Our results indicate that for TCRαβ$^+$CD8αα$^+$ T-IEL, this rewiring most likely occurs post-selection in the thymus. T-IEL precursors pass through the DP stage (*47*), where high expression of LAT was seen, and only after agonist selection, when T-IEL progenitors downregulate CD4 and CD8 expression, and upregulate TCRβ and CD5 expression, is LAT expression lost. Potentially, strong TCR signals in the absence of costimulation lead to the downregulation of LAT, and to the concomitant expression of several non-T cell proteins, such as LAT2, Lyn, CLNK, and GCSAM, that are normally expressed in B cells. Several of these proteins were also shown to define the transcriptional profile of human agonist-selected CD8αα$^+$ T-IEL precursors in the thymus, e.g., GCSAM, DUSP6, LYN, CLNK, among others (*48*). Of note, forced expression of LAT in bone marrow progenitors blocks B cell development. Hence, we propose that in T-IEL, LAT drives the expression of some transcriptional regulator that represses B cell lineage proteins, whereas loss of LAT permits their re-expression. This reprogramming of T-IEL for tolerance induction is a deliberate process during selection, and not just the escape of a few clones from negative selection. Interestingly, this mechanism of tolerance induction may be specific to agonist-selected T-IEL, as loss of LAT adversely affects Treg survival and function (*45*).

Surprisingly, negative regulators of signaling, including SHP-1/2, LAT2, and LAG-3 did not play a major role in regulating T-IEL responses. LAT2 was a promising candidate, as it is highly expressed in natural T-IEL and is believed to compete with LAT for binding to downstream signaling proteins (*49*), thus reducing signal transduction through LAT. Yet we found only marginally improved functional responses in T-IEL in the absence of LAT2. It has previously been hypothesized that signaling through inhibitory receptors could keep T-IEL in check. However, loss of key inhibitory phosphatases SHP-1 and SHP-2 had absolutely no effect on T-IEL in homeostasis and in the context of TCR stimulation. This is in line with recent data showing that loss of SHP-1/SHP-2 also had no effect on T cell anti-tumor responses (*50*). In our phospho-proteomic analyses we identified several less explored receptors, such as CD244/2B4 and CD200R1. Both CD200R1 and 2B4 have been shown to downmodulate responses to TCR stimulation (*36*). However, the ligands for these receptors are not expressed on T-IEL, and the persistent lack of TCR responses in T-IEL cultured in the absence of epithelial cells argue that multiple layers of inhibitory signals may contribute to keeping T-IEL in check, but no one single mechanism is necessary.

Despite our finding that ligation of the TCR does not lead to activation of LAT and conventional downstream signaling pathways in natural T-IEL, we cannot absolutely rule out a role for the TCR in T-IEL function. It is possible that alternative pathways are transduced through the TCR and LAT2, which, in conjunction with other co-stimulatory signals in the intestine, drive T-IEL function. During infection, intestinal epithelial cells could upregulate costimulatory ligands and cytokines while downregulating inhibitory signals that in combination permit T-IEL activation. Like dendritic epidermal T cells in the skin, T-IEL may utilize their TCR as a normality sensor, where loss of the TCR ligand(s) on epithelial cells triggers an alarm signal for the activation of T-IEL (*51*). However, it is clear that the TCR on T-IEL is not constitutively transducing strong signals at steady-state, as our data on the NR4A3 reporter, as well as data from the newly made Nur77-Tempo reporter (*52*), that is more sensitive to TCR signals, show activity of the TCR in T-IEL only in a small subset at steady-state. Our data, alongside other studies showing that the TCR was also shown not be required for the survival and maintenance of an induced T-IEL subset, the TCR$\alpha\beta^{+}$CD8$\alpha\beta^{+}$ subset (*15*), clearly indicate limited TCR activity in T-IEL at steady-state.

In this study we mainly focus on agonist selected TCRαβ^{+}CD8αα^{+} T-IEL and show that during development, the TCR of these self-reactive T cells is rendered hyporesponsive by switching off expression of the adaptor protein LAT. However, loss of LAT may be a mechanism of switching off the TCR in other innate-like lymphocytes to prevent autoreactivity, such as γδ T-IEL, as we show here, and in skin dendritic epidermal γδ T cells, and CD27- γδ T cells. The loss of TCR reactivity may further allow these T cell responses to be driven by other activating receptors and cytokines. Based on our findings, we suggest that the rewiring of the TCR signalosome is a novel mechanism for driving tolerance or anergy of autoreactive T cells, that may apply to other T cell types.

Author contributions

MS conceptualized and designed the study, HJW, ASC, FL, SP, EK, KDR, DB, MS performed experiments and analyzed data. HJW and MS prepared figures and wrote the manuscript with input from all co-authors.

Acknowledgements

We are very grateful to Dr. I. Moraga for help with fluorescent cell barcoding set up and analysis, Dr. S. Schattgen for reanalysis of human scRNA-seq data, and Profs. D. Cantrell and Y. Kulathu at the University of Dundee and Prof. S. Minguet, University of Freiburg, for many useful discussions. We acknowledge the contribution of Dr. V Bugajev and Prof. Petr Draber (Prague, Czech Republic) for initial analyses of the LAT2 KO mice. We would like to thank A. Rennie and R. Clarke for cell sorting, the staff of the Biological Resource Unit for technical assistance, and the mass spectrometry facility at the MRC Protein Phosphorylation and Ubiquitylation Unit. EK and KDR are funded by a Cancer Research UK fellowship to KDR (C66224/A27092). DB is funded by an MRC Career Development Award (MR/V009052/1) and a Lister Institute Fellowship. HJW, ASC and MS are funded by the Wellcome Trust, FL and SP are supported by the Medical Research Council UK funding to the MRC PPU, and MS is also supported by the EMBO Young Investigator Programme.

Funding

This research was funded by a Wellcome Trust PhD studentship to HW (222320/Z/21/Z) and by the Wellcome Trust and Royal Society Sir Henry Dale Fellowship to MS (206246/Z/17/Z). For the purpose of open access, the authors have applied a CC BY public copyright licence to any Author Accepted Manuscript version arising from this submission.

Declaration of interests: The authors declare no conflicts of interest.

Methods

Mice

Mice were bred and maintained with approval by the University of Dundee ethical review committee under a UK Home Office project license (PD4D8EFEF, PP2719506) in compliance with UK Home Office Animals (Scientific Procedures) Act 1986 guidelines. C57BL/6J mice were purchased from Charles River and acclimatized for at least 7 days prior to use. Ly5.1 mice were purchased from Charles River and bred in house. *Lat2*$^{-/-}$ (LAT2 KO) mice were obtained from Prof. Petr Draber (Prague, Czech Republic) under MTA from Prof. Bernard Malissen (Marseilles, France). *Ptpn6*$^{fl/fl}$ (JAX stock #008336) or *Ptpn6*$^{fl/fl}$/*Ptpn11*$^{fl/flBgn}$ mice (50) were obtained from Doreen Cantrell, University of Dundee and crossed to *GzmB*$^{Cre/+}$ (Gzmb-Cre knockin) mice that were generated by Ingenious Targeting Laboratory for MS. This resulted in generation of GzmB-Cre/ *Ptpn6*$^{fl/fl}$ and GzmB-Cre/ *Ptpn6*$^{fl/fl}$/*Ptpn11*$^{fl/fl}$ mice that had deletion of SHP-1 (*Ptpn6*) alone or SHP-1 and SHP-2 (*Ptpn6* and *Ptpn11*) in all Granzyme B expressing cells. As T-IEL highly express Granzyme B, *Ptpn6* and/or *Ptpn11* were deleted in these cells. Mice were maintained in a standard barrier facility on a 12hr light/dark cycle at 21°C in individually ventilated cages with sizzler-nest material and fed an R&M3 diet (Special Diet Services, UK) and filtered water ad libitum. Cages were changed at least every 2 weeks. Nr4a3-Tocky mice were obtained under MTA with Dr. Masahiro Ono (Imperial College London, UK) and were bred and maintained at the University of Birmingham under UK Home Office Project Licence P18A92E0A.

Isolation of Intestinal Intraepithelial T Lymphocytes

T-IEL were isolated as previously described (James, Vandereyken et al. 2020). Briefly, the small intestine was removed and flushed with PBS. The intestine was cut longitudinally and then transversely into 0.5 cm pieces. Gut pieces were incubated in RPMI containing 10% FBS, Penicillin/Streptomycin, L-Glutamine and 1 mM DTT. After 40-minute incubation with shaking, pieces of gut were vortexed and filtered through a 100 µm cell strainer. Filtrate was spun and resuspended in 44% Percoll. This was layered on top of 75% Percoll (Sigma) and spun at 700g for 30 minutes without brake. Cells were removed from the interface of the Percoll layers and washed before further use.

Isolation of thymocytes, splenocytes and lymph node cells

Thymus, spleen or inguinal, mesenteric, brachial, axillary and cervical lymph nodes were removed from mice and crushed through a 70 µm cell strainer into isolation media. Cell suspensions resuspended in appropriate buffer for downstream application.

Stimulation and Fluorescent Cell Barcoding with Live/Dead dyes

T-IEL were isolated and sorted with the CD8a Positive Selection Kit (Stemcell Technologies) and stained with Live/Dead Near-Infrared (ThermoFisher Scientific) then resuspended in stimulation media at 1 x 10^6 cells/ml. Lymph node CD8α$^+$ T cells were isolated and sorted using the CD8α Positive Selection Kit (Stemcell Technologies). Isolated cells were washed and resuspended at 1 x 10^6 cells/ml in stimulation media. Stained T-IEL and unstained lymph node T cells were mixed at a 1:1 ratio before stimulation with 30 µg/ml anti-CD3 (Clone 145-2C11, Biolegend) crosslinked with 5 µg/ml anti-Hamster (Jackson Immunoresearch). PP2 was added at 20 µM, GDC-0941 at 1 µM and Rapamycin at 20 nM to relevant condition for 1 hour prior to stimulation, pervanadate was used at 10 µM. PMA was used at 100 ng/ml and ionomycin at 1 µg/ml. During stimulation cells were incubated at 37°C on shaking incubator, 400 rpm. Cells were fixed in 2% paraformaldehyde (PFA), incubated for 10 minutes, and permeabilised with 90% ice cold methanol.

After permeabilization, the different stimulation conditions were subject to barcoding with different concentrations of Pacific Blue NHS ester dye or Pacific Orange succinimidyl ester (both ThermoFisher Scientific). Barcoded conditions were pooled and then subject to further intracellular and surface staining.

Phospho-flow cytometry

Fixed and permeabilised cells were incubated with primary phospho-antibodies; Phospho-CD3ζ (Y142) (Clone K25-407.69), Phospho-SLP-76 (Y128) (Clone J141-668.36.58) (both BD Biosciences); Phospho-ZAP-70 (Y319)/Syk (Y352) (Clone 65 E4), Phospho-ERK1/2 (T202/Y204) (Clone 197G2), Phospho-Akt (S473) (Clone 193H12), Phospho-S6 ribosomal protein (S235/236) (Clone D57.2.2E), Phospho-4EBP1 (T37/46) (Clone 236B4), Phospho-CREB (S133) (Clone 87G3), Phospho-p38 MAPK (T180/Y182) (Clone D3F9), P-Akt (T308) (Clone D25E6), Phospho-p70 S6 kinase (T389), Phospho-PI3K p85 (Y458)/p55(Y199) (all Cell Signaling

Technology). Primary antibodies were incubated for 30 minutes at room temperature in the dark before incubation with secondary antibody, anti-rabbit Dylight649 (Biolegend) or Alexa Fluor 647 AffiniPure $(Fab')_2$ Fragment Donkey Anti-Mouse IgG (H+L) (Jackson ImmunoResearch). Secondary antibody was incubated for 30 minutes at room temperature in the dark before washing and incubation with surface stains; TCRβ-PE (Clone H57-587) and CD8α-PE-Cy7 (Clone 53-6.7) (both Biolegend); TCRγδ-PerCP efluor710 (Clone GL3) and CD8β-FITC (Clone H35-17.2) (both eBioscience). After incubation, cells were washed and read on Cytoflex (Beckman Coulter).

Flow cytometry

Intracellular staining was performed on cells isolated as described above that were stained with Live/Dead Fixable Near-InfraRed or Live/Dead Fixable Blue (1:1000) (ThermoFisher Scientific) and fixed and permeabilised using the Fixation/Permeabilisation and Permeabilisation buffers (eBiosciences) following manufacturers protocols. Permeabilised cells were stained with antibodies, TCR Vγ7 (1:100) (Biolegend) followed by anti-mouse PE (Biolegend), LAT (1:200), SHP-1 or SHP-2 (all Cell Signaling Technology) followed by anti-rabbit Dylight649 (1:500) (Biolegend), NTAL-PE (1:100) (ThermoFisher Scientific).

Surface staining was performed on cells. Antibodies used were CD1d-APC (???), CD4-BV605 (1:400), CD8α-AF700 (1;400), CD5-PE-Cy7 (1:400), CD25-APC (1:100), LAG-3-PE-Cy7 (1:200) (all Biolegend) and TCRβ-BV786 (1:200) (BD Biosciences).

T-IEL isolated from untreated Nr4a3-Tocky mice or mice that were injected with anti-CD3 (Clone 145-2C11) or IgG (both Biolegend) were stained with Viability dye-efluor780 (eBiosciences), then TCRβ- AF700 (Clone H57-597), TCRγδ-APC (Clone CL3), CD8β-PerCP-Cy5.5 (Clone 53-5.8) (all Biolegend); CD8α-BUV395 (Clone S3-6.7) and CD4-BUV737 (Clone GK1.5) (both BD Biosciences). Fluorescence of Nr4a3-blue and Nr4a3-red in all T cell subsets was ascertained by flow cytometry.

Cytokine production upon *in vivo* stimulation with anti-CD3

Mice were treated with 50 µg anti-CD3 Ultra-LEAF (Clone 145-2C11) (Biolegend) or sterile PBS (Gibco) for 3 hours prior to harvesting T-IEL and spleen. Tissues were processed following protocols described above. Cells

were treated with Brefeldin A and GolgiStop (both Biolegend) for 2 hours prior to fixation and permeabilisation with 1X Fixation/Permeabilisation buffer and 1X Permeabilisation buffer (eBiosciences). Cells were stained with TNFα-PE (1:200), IFNγ-PE Dazzle594 (1:200), CD8α-PE-Cy7 (1:400), CD8β-FITC (1:400) and CD4-BV605 (1:400) (all Biolegend), TCRβ-BV786 (1:200), TCRγδ-PerCP-ef710 (1:200) (both BD Biosciences). Cells were acquired on LSR Fortessa.

T-IEL Cultures

T-IEL were isolated and purified using the CD8α Positive Selection kit (StemCell Technologies) following manufacturers instructions. Cells were resuspended in RPMI(Gibco) supplemented with 10% FBS, penicillin, streptomycin, 2 mM L-Glutamine, 1 mM sodium pyruvate, 1 mM β-mercaptoethanol, 2.5 mM HEPES and 1% non-essential amino acids. IL-15/IL-15Rα (ThermoFisher Scientific) was added at 100ng/ml. Anti-LAG-3 (Clone C9B7W) was used at 10 μg/ml.

Degranulation assay

T-IEL were isolated and purified using the CD8α Positive Selection kit (StemCell Technologies) following manufacturers instructions. Cells were cultured as indicated before plating at $1x10^6$ cells/ml in culture media supplemented with 100 ng/ml IL-15/IL-15Rα, Brefeldin A (Biolegend), BD GolgiStop (BD Biosciences), CD107a (1D4B) and CD107b (M3/84) (both Biolegend). Cells were plated in a 96-well round-bottom plate coated with 3 μg/ml anti-CD3 (Biolegend), uncoated well or with PMA (1 ng/ml) and Ionomycin (1 μg/ml). Cells were harvested after 4 hours. Those assessed for signaling proteins were stained as described in the 'Phospho-flow cytometry' section. Cells to be assessed for degranulation were fixed with Fixation/Permeabilization Concentrate and permeabilised with Permeabilisation buffer (eBiosciences). Cell were then stained for IFNγ-PE/Dazzle 594 (CloneXMG1.2) (Biolegend). Cells were measured on LSR Fortessa (BD Biosciences).

Sample preparation for Phospho-proteomics

T-IEL and lymph node cells were isolated following the previously described method. CD4 and CD8β cells were depleted from the T-IEL compartment using CD4 and CD8β biotinylated antibodies and magnetic streptavidin nanobeads (MojoSort) (Biolegend). $CD8\alpha^+$ cells were purified from CD4 and CD8β depleted T-IEL

and lymph node T cells using the CD8α Positive Selection Kit (Stemcell Technologies). Cells were resuspended in RPMI + 1% FBS + L-Glutamine + Pen/Strep at a concentration of $1x10^6$ cells/ml and stimulated with 10 µM of pervanadate. After 5 minutes cells were pelleted and snap-frozen. Cells were lysed with 5% sodium dodecyl sulphate + 50 mM triethylammonium bicarbonate (TEAB) (Sigma). Samples were lysed by rounds of shaking at 1000 rpm at room temperature and at 95°C at 500 rpm and sonication. Benzonase was added and incubated for 15 minutes at 37°C. Samples were prepared following the S-trap mini protocol (Protifi). Briefly, lysates were reduced using 10 mM TCEP, alkylated with 0.5 M chloracetamide, acidified with 12% phosphoric acid. 300 µg of each sample was loaded onto an S-Trap mini column and digested using trypsin (Sigma) at 1:20 wt:wt. Samples were eluted from the column and vacuum dried using SpeedVac. Samples were subject to C18 Clean up (Waters) and labelling with 10 plex Tandem Mass Tagging Kit (ThermoFisher Scientific) following manufacturers protocols. Labelled samples were combined and Vacuum dried. Samples were resuspended in 50 mM ammonium bicarbonate and incubated with SH2 superbinder beads (Precision Proteomics). After 1 hour of incubation beads were washed thoroughly with ammonium bicarbonate. Beads were resuspended in 0.4% trifluoroacetic acid (TFA) then passed through a Spin-X column (Corning). Samples were vacuum dried before resuspension in formic acid and injection onto the mass spectrometer.

Fractionation

The quenched samples were then mixed and fractionated with high pH reverse-phase C18 chromatography using the Ultimate 3000 high-pressure liquid chromatography system (Thermo Scientific) at a flow rate of 500 µl/min using two buffers: buffer A (10 mM ammonium formate, pH 10) and buffer B (80% ACN, 10 mM ammonium formate, pH 10). Briefly, the TMT-labelled samples were resuspended in 200 µl of buffer A and desalted then fractionated on a C18 reverse-phase column (4.6 × 250 mm, 3.5 µm, Waters) with a gradient as follows: 3% Buffer B for 19 min at 275 µl/min (desalting phase), ramping from 275 µl/min to 500 µl/min in 1 min, 3% to 12% buffer B in 1 min, 12% to 40% buffer B in 30 min, 40% B to 60% B in 5 min, 60% B to 95% B in 2 min, 95% for 3 min, ramping to 3% B in 1 min and then 3% for 9 min. A total of 96 fractions were collected and then concatenated into 12 fractions, which were further speed vacuum-dried prior to LC–MS/MS analysis.

Samples (12 Fractions and the pooled sample) were resuspended in 5% formic acid in water and injected on an UltiMate 3000 RSLCnano System coupled to an Orbitrap Fusion Lumos Tribrid Mass Spectrometer (Thermo Scientific). Peptides were loaded on an Acclaim Pepmap trap column (Thermo Scientific #164750) prior analysis on a PepMap RSLC C18 analytical column (Thermo Scientific #ES903) and eluted on a 120 min linear gradient from 3 to 35% Buffer B (Buffer A: 0.1% formic acid in water, Buffer B: 0.08% formic acid in 80:20 acetonitrile:water (v:v)). Eluted peptides were then analysed by the mass spectrometer operating in Synchronous Precursor Selection mode using a cycle time of 3s. MS1 were acquired at a resolution of 120000 with an AGC target of 100% and a maximum injection time of 50 ms. Peptides were then selected for MS2 fragmentation using CID with an isolation width of 0.7 Th, NCE of 35%, AGC of 100% and maximum injection time of 50 ms using the “rapid” scan rate. Up to 10 fragments were then selected for MS3 fragmentation using HCD with an isolation width of 3 Th, NCE of 65%, AGC of 200% and maximum injection time of 105 ms and spectra were acquired at a resolution of 50000. Dynamic exclusion was set to 60 s with a tolerance of +/- 10 ppm.

Mass Spectrometry Data Analysis

Peptides were searched against Uniprot Swissprot Mouse containing isoforms (released on 2023/01/02) using MaxQuant (v2.2.0.0) [see reference below]. All parameters were left as default except for the addition of Deamidation (N, Q) and Phospho (S, T, Y) as variable modifications modification and the inclusion of MS3 TMT quantitation. Statistical analysis was carried out using Python (v3.9.0) and packages pandas (v1.3.3), numpy (v1.19.0), sklearn (v1.0), scipy (v1.7.1), rpy2 (v3.4.5), Plotnine (v0.7.1) and Plotly (v5.8.2) and R (v4.1.3) and the package Limma (3.50.1) [see reference below]. Sites identified as reverse, potential contaminant or with a localization confidence lower than 0.75 and sites quantified in less than 3 replicates in at least 1 condition were excluded. Missing values were then imputed using a gaussian distribution centred on the median with a downshift of 1.8 and width of 0.3 (relative to the standard deviation). Protein regulation was assessed using LIMMA and P-values were adjusted using Benjamini Hochberg multiple hypothesis correction. Proteins were considered significantly regulated if their corrected P-value was smaller than 0.05 and their fold change was greater than 2 or smaller than 1/2. Data analysis was carried out using R (v4.2.3). Phospho-proteomic heatmaps were made using Morpheus (Broad Institute).

MaxQuant: https://www.nature.com/articles/nbt.1511

Limma: https://academic.oup.com/nar/article/43/7/e47/2414268

Morpheus: https://software.broadinstitute.org/morpheus

Retroviral Transduction of T-IEL and LSK cells

Phoenix-Eco cells were maintained in DMEM (Gibco), 10% FBS, 1X Penicilin/Streptomycin, 1X pyruvate. $3x10^6$ cells were plated 24 hours prior to being transfected with 10 µg of either pMSCV-IRES-GFP or pMSCV-LAT-IRES-GFP combined with 10 µg of the packaging plasmid pCL-Eco using the calcium phosphate method. Briefly, the packaging plasmid was combined with the pCL-Eco plasmid, 50 µl CaCl2 and deionised water to a volume of 500 µl. 500 µl 2X HBS (140 mM NaCl, 1.5 mM Na2HPO4, 50 mM HEPES, pH 7.05) was added dropwise to the mixture while vortexing. The transfection mix was added dropwise to the Phoenix cells. Media was refreshed 12 – 16 hours after transfection. 48 hours after transfection virus was harvested and filtered through a 0.45 µm filter. Media was refreshed on the Phoenix cells and virus harvested at 72 hours post-transfection.

To isolate hematopoietic stem and progenitor cells (HSPCs), femur, tibia and hip bones were taken from Ly5.1 mice and crushed using a mortar and pestle into PBS containing 2% FBS. Cell suspension was filtered through a 70 µm cell strainer. Red blood cells were lysed by incubation in ACK buffer for 2 minutes. Lineage cells were depleted using the Direct Lineage Depletion Kit (Miltenyi). Cells were stained for Lineage markers; CD3, B220, Ter119, CD11b and Ly6G all PE-Cy5 (BD Biosciences), Sca-1-PE (BD Biosciences) and cKit-APC-Cy7 (Biolegend). Lineage-negative, Sca-1+cKit+ (LSK) cells were sorted using a MA900 Cell Sorter (Sony Biosciences). LSK cells were stimulated for 48 hours in serum-free conditions (50% StemPro™-34 (Gibco), 50% IMDM+GlutaMAX (Gibco), StemPro™ supplement (Gibco), Penicillin/Streptomycin, L-Glutamine, 75 µM 1-Thioglycerol (Sigma-Aldrich), 25 U/ml Heparin (Sigma-Aldrich), 10 ng/ml mFGF (Peprotech), 20 ng/ml mIGF II (R&D Systems), 40 ng/ml TPO (Peprotech) and 10 ng/ml SCF (Peprotech) in non TC treated plates. T-IEL were harvested following the previously described protocol. 48 hours after isolation, the cells were transduced with virus. Plates were coated with Retronectin (TakaraBio) and filtered supernatant of Phoenix cells producing virus loaded by two rounds of centrifugation. Cells were added to the plates containing the virus bound onto the retronectin and

spun briefly. Cells were incubated at 37°C overnight and the transduction process was repeated the following day.

Transduced T-IEL were stimulated following the stimulation protocol described above.

Transfer of Transduced HSPCs into irradiated mice

24 hours before transfer of HSPCs, Ly5.2 mice were irradiated with a total dose of 9.5 Gy fractionated into 4.75 Gy + 4.75 Gy with at least 4 hours interval between doses. Transduced Ly5.1 HSPCs were harvested and combined with whole bone marrow extract from Ly5.2 mice. Between 90,000 and 140,000 transduced HSPCs cells were combined with 100,000 nucleated Ly5.2 bone marrow helper cells and injected into the tail-vein of irradiated recipients. Mice were maintained for 6 weeks before harvest of thymus, spleen and T-IEL compartments.

Data analysis

Flow cytometry data was analyzed using FlowJo Software (v10.9.0). Data analysis and statistical tests were carried out using GraphPad Prism (v10.0.0).

References

1. Joannou K, Baldwin TA. Destined for the intestine: thymic selection of TCRαβ CD8αα intestinal intraepithelial lymphocytes. Clinical and Experimental Immunology. 2023 Jul 1;213(1):67–75.

2. Stritesky GL, Jameson SC, Hogquist KA. Selection of Self-Reactive T Cells in the Thymus. Annual Review of Immunology. 2012 ;30(1):95–114.

3. Vahl JC, Heger K, Knies N, Hein MY, Boon L, Yagita H, et al. NKT Cell-TCR Expression Activates Conventional T Cells in Vivo, but Is Largely Dispensable for Mature NKT Cell Biology. Marrack P, editor. PLoS Biol. 2013 Jun 18 ;11(6):e1001589.

4. Vahl JC, Drees C, Heger K, Heink S, Fischer JC, Nedjic J, et al. Continuous T Cell Receptor Signals Maintain a Functional Regulatory T Cell Pool. Immunity. 2014 Nov;41(5):722–36.

5. McDonald BD, Jabri B, Bendelac A. Diverse developmental pathways of intestinal intraepithelial lymphocytes. Nat Rev Immunol. 2018 Aug;18(8):514–25.

6. Guy-Grand D, Vassalli P, Eberl G, Pereira P, Burlen-Defranoux O, Lemaitre F, et al. Origin, trafficking, and intraepithelial fate of gut-tropic T cells. J Exp Med. 2013 Aug 26;210(9):1839–54.

7. Leishman AJ, Gapin L, Capone M, Palmer E, MacDonald HR, Kronenberg M, et al. Precursors of Functional MHC Class I- or Class II-Restricted CD8αα+ T Cells Are Positively Selected in the Thymus by Agonist Self-Peptides. Immunity. 2002 Mar;16(3):355–64.

8. Pobezinsky LA, Angelov GS, Tai X, Jeurling S, Van Laethem F, Feigenbaum L, et al. Clonal deletion and the fate of autoreactive thymocytes that survive negative selection. Nat Immunol. 2012 Jun;13(6):569–78.

9. Ruscher R, Kummer RL, Lee YJ, Jameson SC, Hogquist KA. CD8αα intraepithelial lymphocytes arise from two main thymic precursors. Nat Immunol. 2017 Jul;18(7):771–9.

10. McDonald BD, Bunker JJ, Ishizuka IE, Jabri B, Bendelac A. Elevated T cell receptor signaling identifies a thymic precursor to the TCRαβ(+)CD4(-)CD8β(-) intraepithelial lymphocyte lineage. Immunity. 2014 Aug 21;41(2):219–29.

11. Mayans S, Stepniak D, Palida S, Larange A, Dreux J, Arlian B, et al. αβT cell receptors expressed by CD4(-)CD8αβ(-) intraepithelial T cells drive their fate into a unique lineage with unusual MHC reactivities. Immunity. 2014 Aug 21;41(2):207–18.

12. Ruscher R, Lee ST, Salgado OC, Breed ER, Osum SH, Hogquist KA. Intestinal CD8αα IELs derived from two distinct thymic precursors have staggered ontogeny. J Exp Med. 2020 Aug 3;217(8):e20192336.

13. Hwang JR, Byeon Y, Kim D, Park SG. Recent insights of T cell receptor-mediated signaling pathways for T cell activation and development. Exp Mol Med. 2020 May 21;52(5):750–61.

14. Mosley RL, Whetsell M, Klein JR. Proliferative properties of murine intestinal intraepithelial lymphocytes (IEL): IEL expressing TCRαβ or TCRτδ are largely unresponsive to proliferative signals mediated via conventional stimulation of the CD3-TCR complex. Int Immunol. 1991;3(6):563–9.

15. Bilate AM, London M, Castro TBR, Mesin L, Bortolatto J, Kongthong S, et al. T Cell Receptor Is Required for Differentiation, but Not Maintenance, of Intestinal CD4+ Intraepithelial Lymphocytes. Immunity. 2020 Nov 17;53(5):1001-1014.e20.

16. Malinarich FH, Grabski E, Worbs T, Chennupati V, Haas JD, Schmitz S, et al. Constant TCR triggering suggests that the TCR expressed on intestinal intraepithelial γδ T cells is functional in vivo. Eur J Immunol. 2010 Dec;40(12):3378–88.

17. Wencker M, Turchinovich G, Di Marco Barros R, Deban L, Jandke A, Cope A, et al. Innate-like T cells straddle innate and adaptive immunity by altering antigen-receptor responsiveness. Nat Immunol. 2014 Jan;15(1):80–7.

18. Di Marco Barros R, Roberts NA, Dart RJ, Vantourout P, Jandke A, Nussbaumer O, et al. Epithelia Use Butyrophilin-like Molecules to Shape Organ-Specific γδ T Cell Compartments. Cell. 2016 Sep 22;167(1):203-218.e17.

19. McDonald BD, Bunker JJ, Ishizuka IE, Jabri B, Bendelac A. Elevated T Cell Receptor Signaling Identifies a Thymic Precursor to the TCRαβ+CD4−CD8β− Intraepithelial Lymphocyte Lineage. Immunity. 2014 Aug;41(2):219–29.

20. Guy-Grand D, Rocha B, Mintz P, Malassis-Seris M, Selz F, Malissen B, et al. Different use of T cell receptor transducing modules in two populations of gut intraepithelial lymphocytes are related to distinct pathways of T cell differentiation. J Exp Med. 1994 Aug 1;180(2):673–9.

21. Ohno H, Ono S, Hirayama N, Shimada S, Saito T. Preferential usage of the Fc receptor gamma chain in the T cell antigen receptor complex by gamma/delta T cells localized in epithelia. The Journal of experimental medicine. 1994 Jan 1;179(1):365–9.

22. Denning TL, Granger SW, Granger S, Mucida D, Graddy R, Leclercq G, et al. Mouse TCRαβ+CD8αα intraepithelial lymphocytes express genes that down-regulate their antigen reactivity and suppress immune responses. J Immunol. 2007 Apr 1;178(7):4230–9.

23. Krutzik PO, Nolan GP. Fluorescent cell barcoding in flow cytometry allows high-throughput drug screening and signaling profiling. Nat Methods. 2006 May;3(5):361–8.

24. Bending D, Martín PP, Paduraru A, Ducker C, Marzaganov E, Laviron M, et al. A timer for analyzing temporally dynamic changes in transcription during differentiation in vivo. Journal of Cell Biology. 2018 Aug 6;217(8):2931–50.

25. Subach FV, Subach OM, Gundorov IS, Morozova KS, Piatkevich KD, Cuervo AM, et al. Monomeric fluorescent timers that change color from blue to red report on cellular trafficking. Nat Chem Biol. 2009 Feb ;5(2):118–26.

26. Jennings E, Elliot TAE, Thawait N, Kanabar S, Yam-Puc JC, Ono M, et al. Nr4a1 and Nr4a3 Reporter Mice Are Differentially Sensitive to T Cell Receptor Signal Strength and Duration. Cell Reports. 2020 Nov;33(5):108328.

27. Brenes AJ, Vandereyken M, James OJ, Watt H, Hukelmann J, Spinelli L, et al. Tissue environment, not ontogeny, defines murine intestinal intraepithelial T lymphocytes. eLife. 2021 Sep 2;10:e70055.

28. Blackburn SD, Shin H, Haining WN, Zou T, Workman CJ, Polley A, et al. Coregulation of CD8+ T cell exhaustion by multiple inhibitory receptors during chronic viral infection. Nat Immunol. 2009 Jan;10(1):29–37.

29. Guy C, Mitrea DM, Chou PC, Temirov J, Vignali KM, Liu X, et al. LAG3 associates with TCR–CD3 complexes and suppresses signaling by driving co-receptor–Lck dissociation. Nat Immunol. 2022 Apr 18;1–11.

30. Cohen G, Makranz C, Spira M, Kodama T, Reichert F, Rotshenker S. Non-PKC DAG/Phorbol-Ester receptor(s) inhibit complement receptor-3 and nPKC inhibit scavenger receptor-AI/II-mediated myelin

phagocytosis but cPKC, PI3k, and PLCγ activate myelin phagocytosis by both. Glia. 2006 Apr 1;53(5):538–50.

31. Chatila T, Silverman L, Miller R, Geha R. Mechanisms of T cell activation by the calcium ionophore ionomycin. J Immunol. 1989 Aug 15;143(4):1283–9.

32. Secrist JP, Burns LA, Karnitz L, Koretzky GA, Abraham RT. Stimulatory effects of the protein tyrosine phosphatase inhibitor, pervanadate, on T-cell activation events. Journal of Biological Chemistry. 1993 Mar 15;268(8):5886–93.

33. Bian Y, Li L, Dong M, Liu X, Kaneko T, Cheng K, et al. Ultra-deep tyrosine phosphoproteomics enabled by a phosphotyrosine superbinder. Nat Chem Biol. 2016 Nov;12(11):959–66.

34. Yao Y, Wang Y, Wang S, Liu X, Liu Z, Li Y, et al. One-Step SH2 Superbinder-Based Approach for Sensitive Analysis of Tyrosine Phosphoproteome. J Proteome Res. 2019 Apr 5;18(4):1870–9.

35. Atlasy N, Bujko A, Bækkevold ES, Brazda P, Janssen-Megens E, Lundin KEA, et al. Single cell transcriptomic analysis of the immune cell compartment in the human small intestine and in Celiac disease. Nat Commun [Internet]. 2022 Aug 22 [cited 2022 Aug 29];13(1):4920. Available from: https://www.nature.com/articles/s41467-022-32691-5

36. Vandereyken M, James OJ, Swamy M. Mechanisms of activation of innate-like intraepithelial T lymphocytes. Mucosal Immunology. 2020 Sep;13(5):721–31.

37. Yasuda T, Bundo K, Hino A, Honda K, Inoue A, Shirakata M, et al. Dok-1 and Dok-2 are negative regulators of T cell receptor signaling. International Immunology . 2007 Apr 1;19(4):487–95.

38. Zhu M, Koonpaew S, Liu Y, Shen S, Denning T, Dzhagalov I, et al. Negative regulation of T cell activation and autoimmunity by the transmembrane adaptor protein LAB. Immunity. 2006 Nov;25(5):757–68.

39. Saito T, Yamasaki S. Negative feedback of T cell activation through inhibitory adapters and costimulatory receptors. Immunological Reviews. 2003 Apr ;192(1):143–60.

40. Brdička T, Imrich M, Angelisová P, Brdičková N, Horváth O, Špička J, et al. Non–T Cell Activation Linker (NTAL). Journal of Experimental Medicine. 2002 Dec 16;196(12):1617–26.

41. Janssen E, Zhu M, Craven B, Zhang W. Linker for activation of B cells: a functional equivalent of a mutant linker for activation of T cells deficient in phospholipase C-gamma1 binding. J Immunol. 2004 Jun 1;172(11):6810–9.

42. Narbona-Sánchez I, Pérez-Linaza A, Serrano-García I, Vico-Barranco I, Fernández-Aguilar LM, Poveda-Díaz JL, et al. Expression of Non-T Cell Activation Linker (NTAL) in Jurkat Cells Negatively Regulates TCR Signaling: Potential Role in Rheumatoid Arthritis. IJMS. 2023 Feb 26;24(5):4574.

43. James OJ, Vandereyken M, Marchingo JM, Singh F, Bray SE, Wilson J, et al. IL-15 and PIM kinases direct the metabolic programming of intestinal intraepithelial lymphocytes. Nat Commun. 2021 Jul 13;12(1):4290.

44. Mingueneau M, Roncagalli R, Grégoire C, Kissenpfennig A, Miazek A, Archambaud C, et al. Loss of the LAT Adaptor Converts Antigen-Responsive T Cells into Pathogenic Effectors that Function Independently of the T Cell Receptor. Immunity. 2009 Aug;31(2):197–208.

45. Shen S, Chuck MI, Zhu M, Fuller DM, Yang C wen O, Zhang W. The Importance of LAT in the Activation, Homeostasis, and Regulatory Function of T Cells. Journal of Biological Chemistry. 2010 Nov ;285(46):35393–405.

46. Schattgen SA, Crawford JC, Van de Velde LA, Chu H, Mazmanian SK, Bradley P, et al. Intestinal Intraepithelial Lymphocyte Repertoires are Imprinted Clonal Structures Selected for MHC Reactivity. SSRN Journal. 2019

47. Hendricks DW, Fink PJ. Uneven Colonization of the Lymphoid Periphery by T Cells That Undergo Early TCRα Rearrangements. The Journal of Immunology. 2009 Apr 1;182(7):4267–74.

48. Verstichel G, Vermijlen D, Martens L, Goetgeluk G, Brouwer M, Thiault N, et al. The checkpoint for agonist selection precedes conventional selection in human thymus. Science Immunology. 2017;12.

49. Roget K, Malissen M, Malbec O, Malissen B, Daëron M. Non-T cell activation linker promotes mast cell survival by dampening the recruitment of SHIP1 by linker for activation of T cells. J Immunol. 2008 Mar 15;180(6):3689–98.

50. Ventura PMO, Gakovic M, Fischer BA, Spinelli L, Rota G, Pathak S, et al. Concomitant deletion of Ptpn6 and Ptpn11 in T cells fails to improve anticancer responses. EMBO Rep. 2022 Nov 7;23(11):e55399.

51. McKenzie DR, Hart R, Bah N, Ushakov DS, Muñoz-Ruiz M, Feederle R, et al. Normality sensing licenses local T cells for innate-like tissue surveillance. Nat Immunol. 2022 Feb 14 ;1–12.

52. Elliot TAE, Jennings EK, Lecky DAJ, Rouvray S, Mackie GM, Scarfe L, et al. Nur77-Tempo mice reveal T cell steady state antigen recognition. Discov Immunol. 2022 Dec 22;1(1):kyac009.